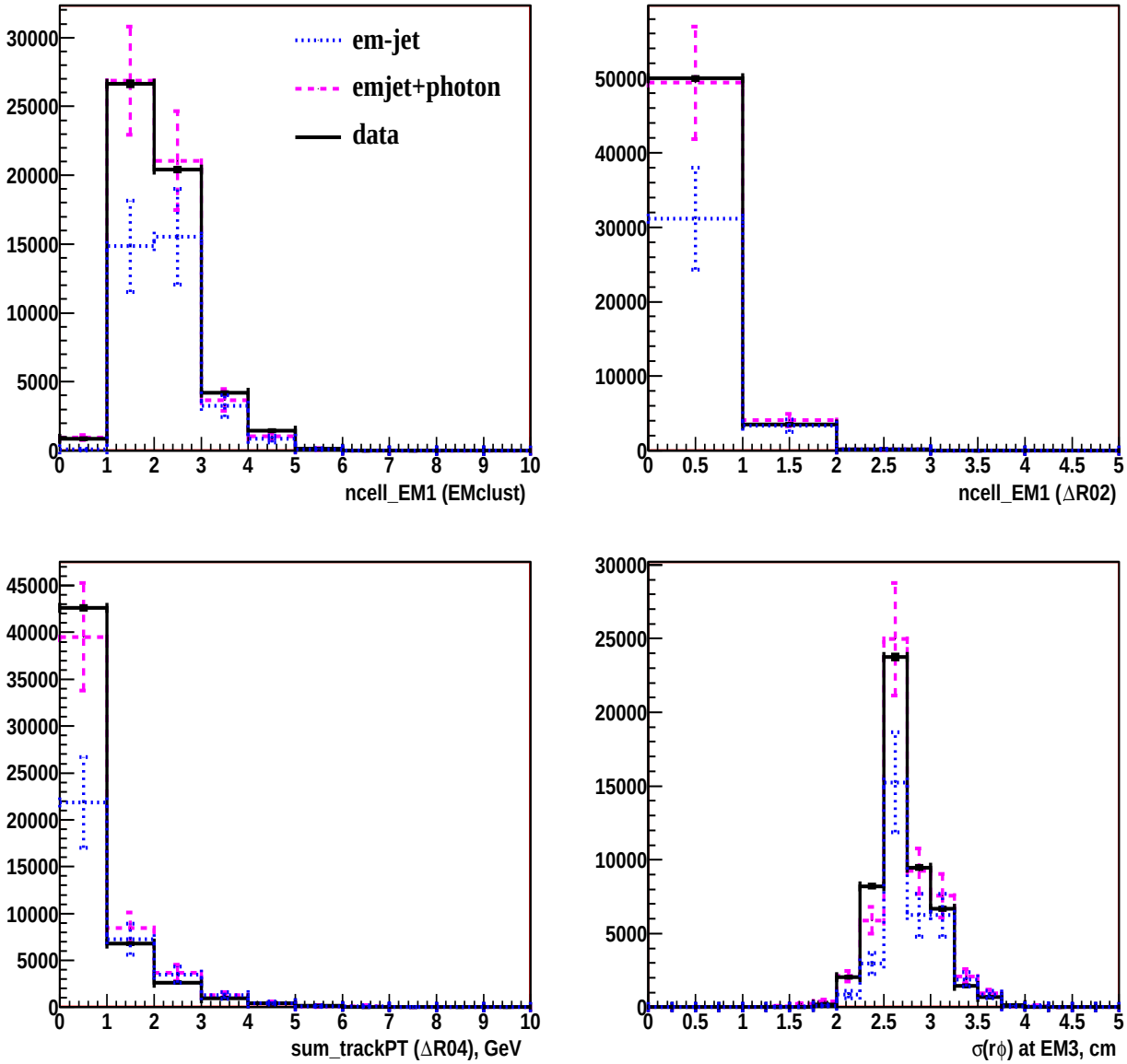

Figure 1: Distribution of the number of events in data and the fitted distributions for MC photons and jets over the four variables used as neural network input vector. MC distributions are weighted with account of their fractions found from the HMCMLL fit. Black histograms (full line) correspond to the data, blue ones (dotted line) to MC em-jets and purple ones (dashed line) to MC total 'em-jet+photons'. All distributions are built after the cut "$NN_{output} > 0.5$" for $\mathbf{23 < p_T^\gamma < 25}$ GeV. The found value of photon purity P for this p_T^γ interval is $P = 0.357 \pm 0.062$.

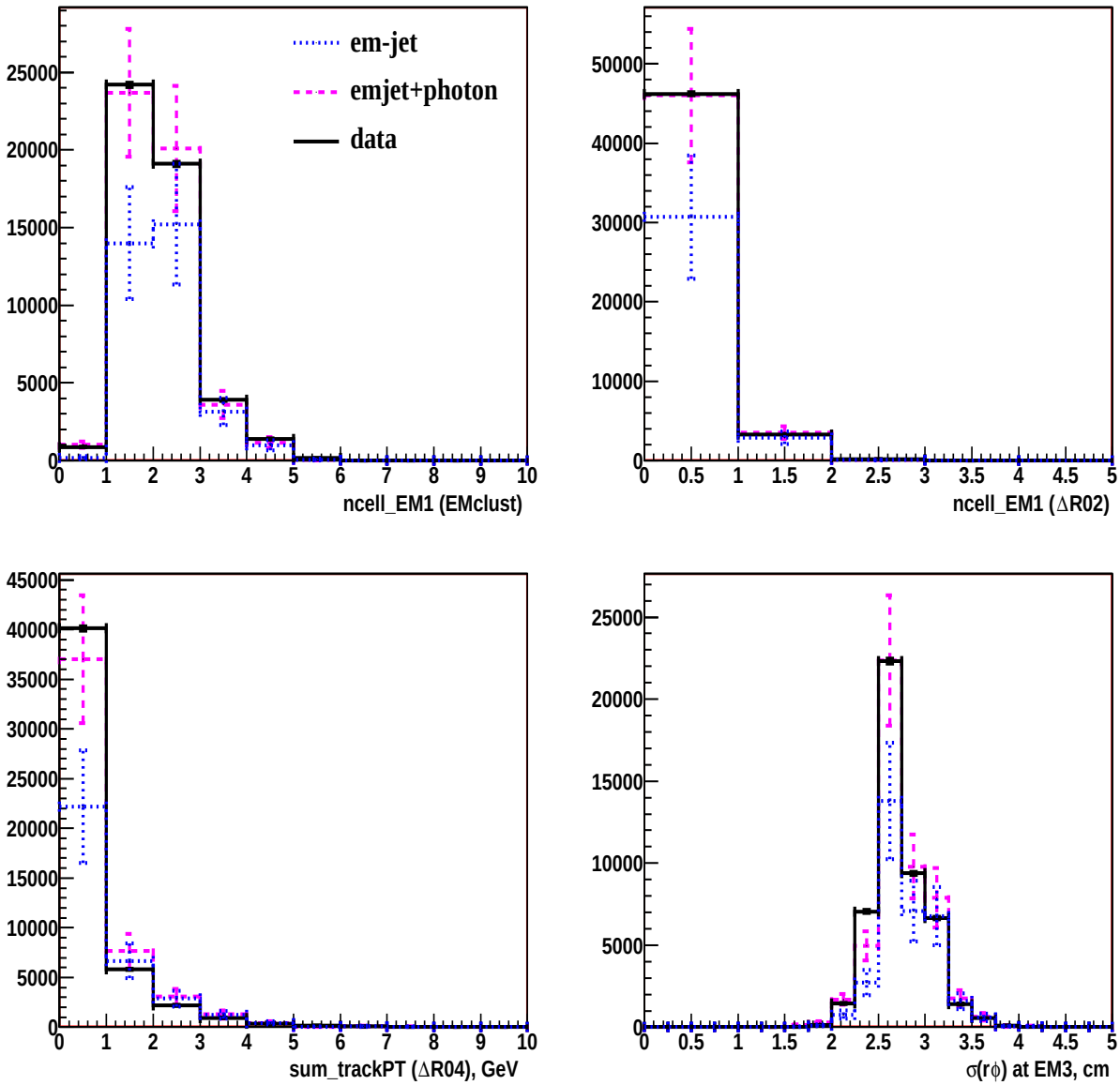

Figure 2: Same as in Fig. 1 but for $\mathbf{25} < \mathbf{p_T^\gamma} < \mathbf{30}$ GeV with $P = 0.346 \pm 0.067$.

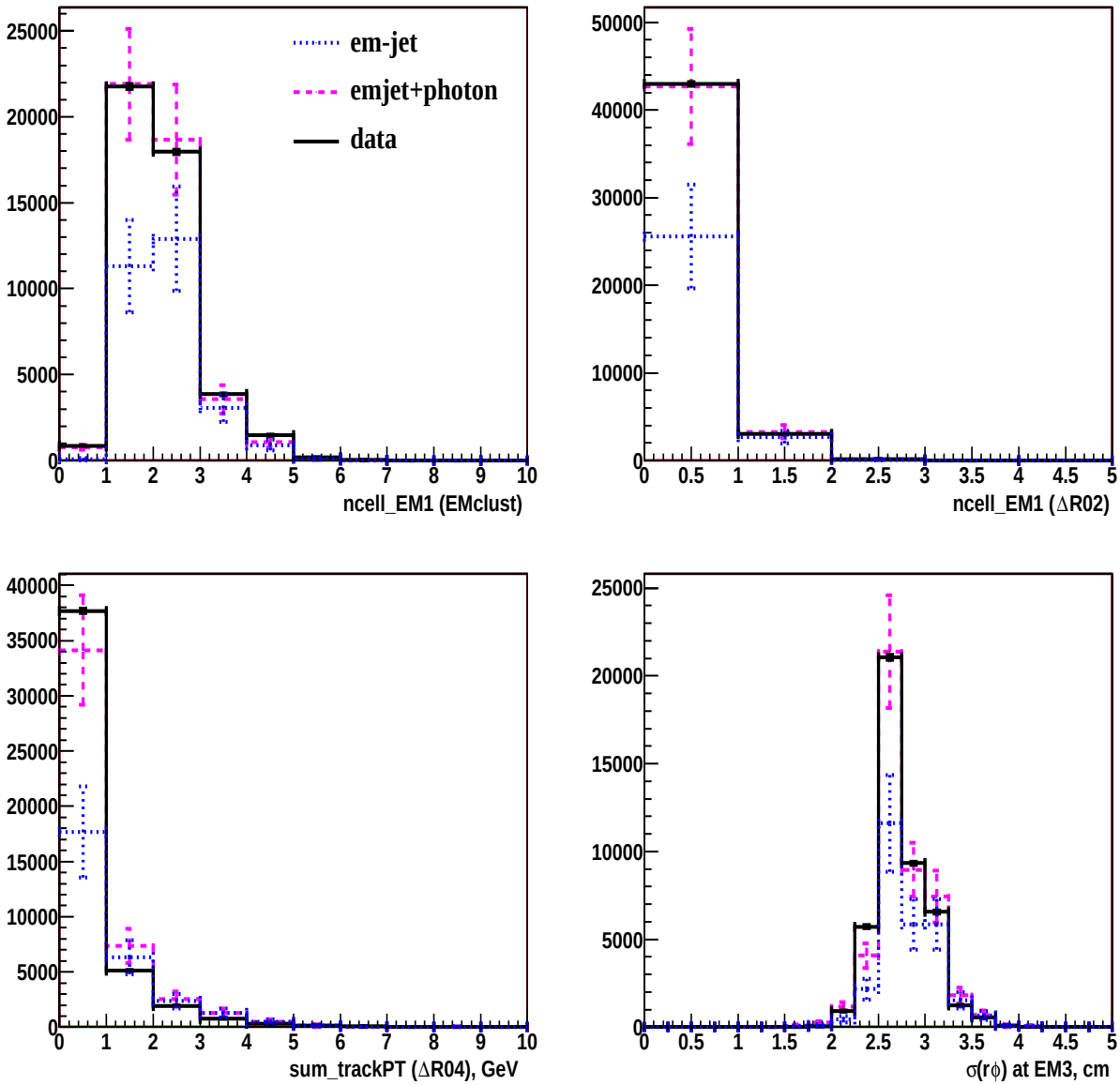

Figure 3: Same as in Fig. 1 but for $\mathbf{30} < \mathbf{p_T^\gamma} < \mathbf{34}$ GeV with $P = 0.384 \pm 0.064$.

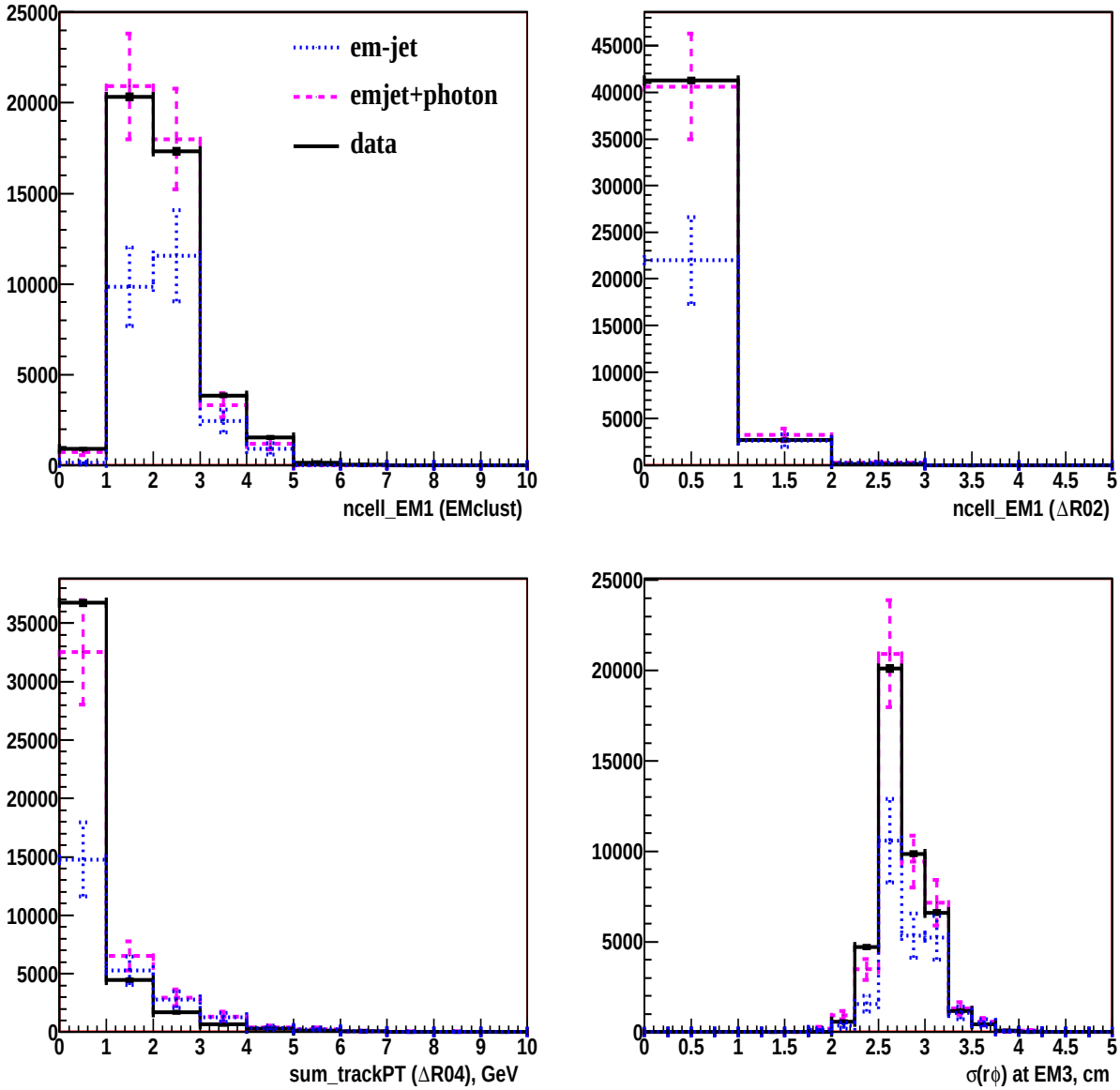

Figure 4: Same as in Fig. 1 but for $\mathbf{34} < \mathbf{p_T^\gamma} < \mathbf{39}$ GeV with $P = 0.436 \pm 0.076$.

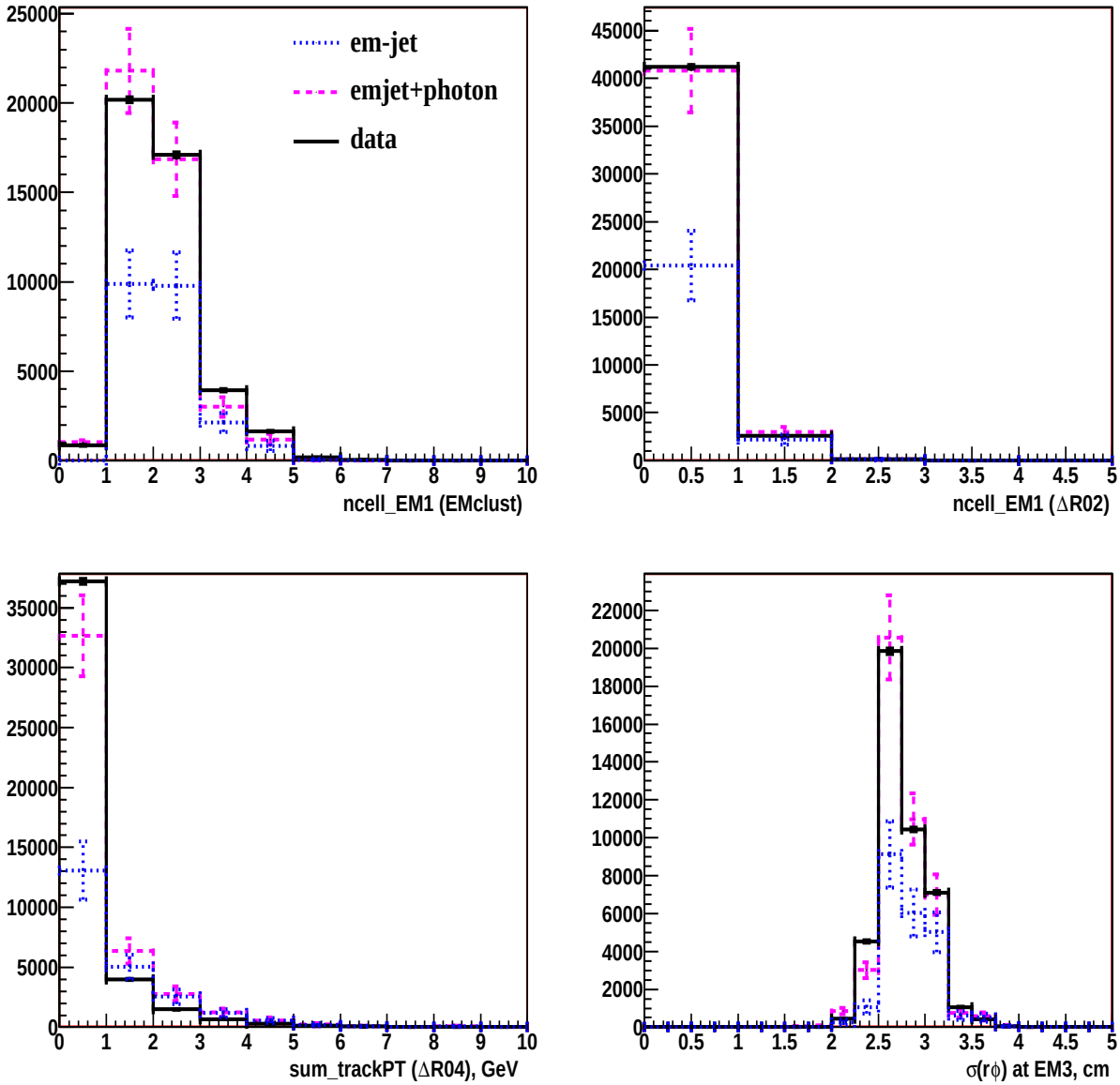

Figure 5: Same as in Fig. 1 but for $\mathbf{39} < \mathbf{p_T^\gamma} < \mathbf{44}$ GeV with $P = 0.484 \pm 0.058$.

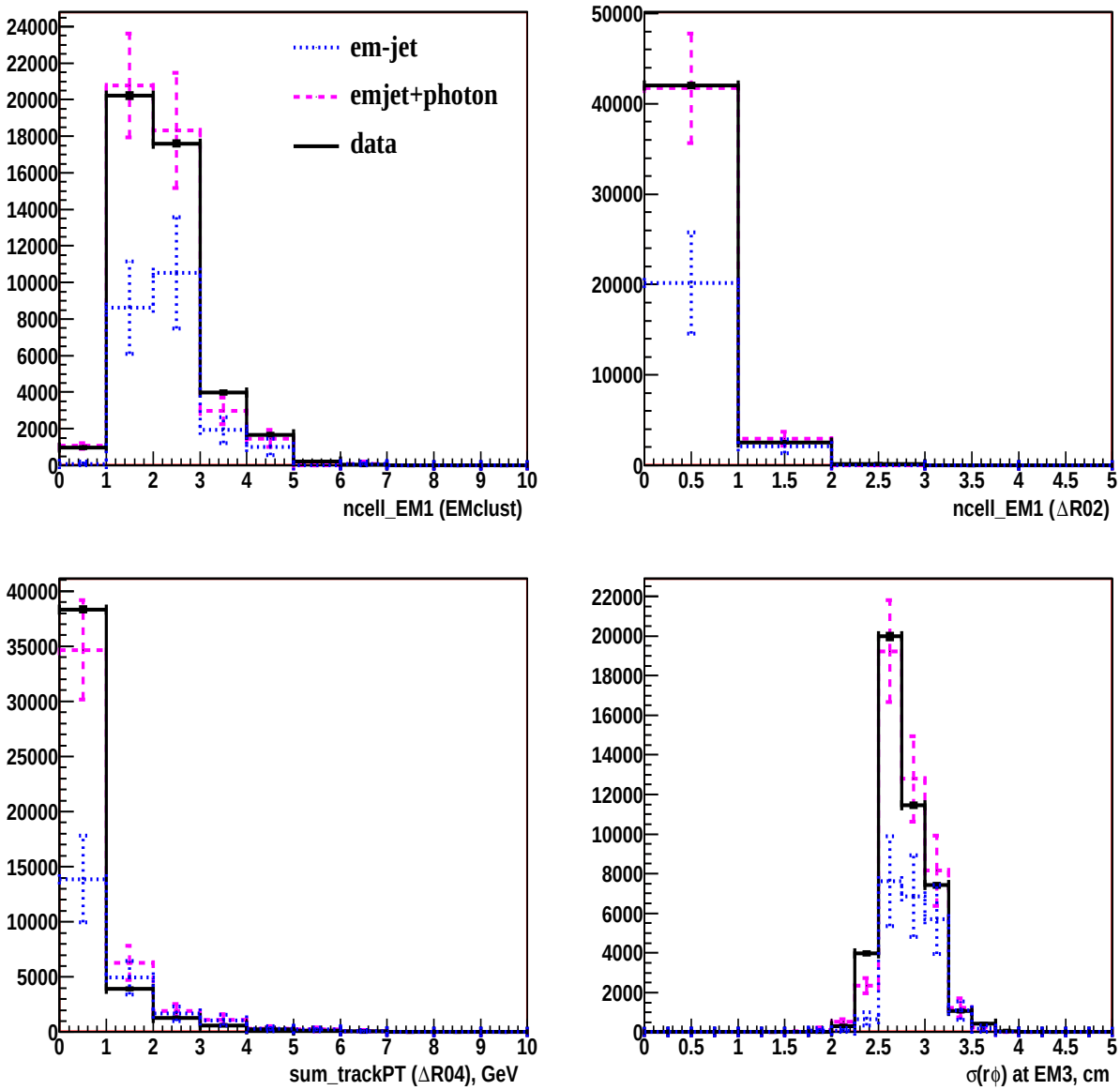

Figure 6: Same as in Fig. 1 but for $\mathbf{44} < \mathbf{p_T^\gamma} < \mathbf{50}$ GeV with $P = 0.512 \pm 0.053$.

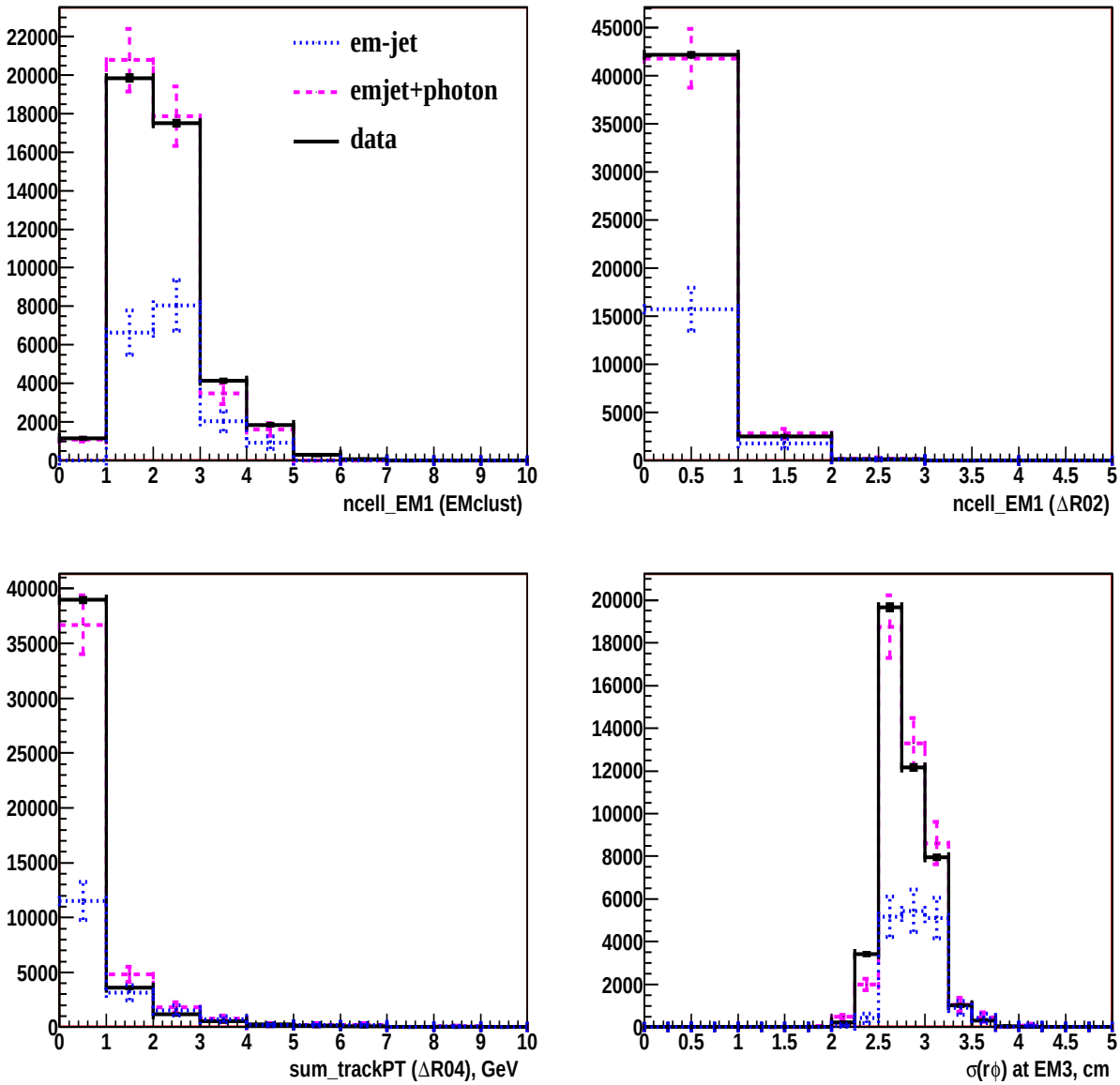

Figure 7: Same as in Fig. 1 but for $\mathbf{50} < \mathbf{p_T^\gamma} < \mathbf{60}$ GeV with $P = 0.607 \pm 0.049$.

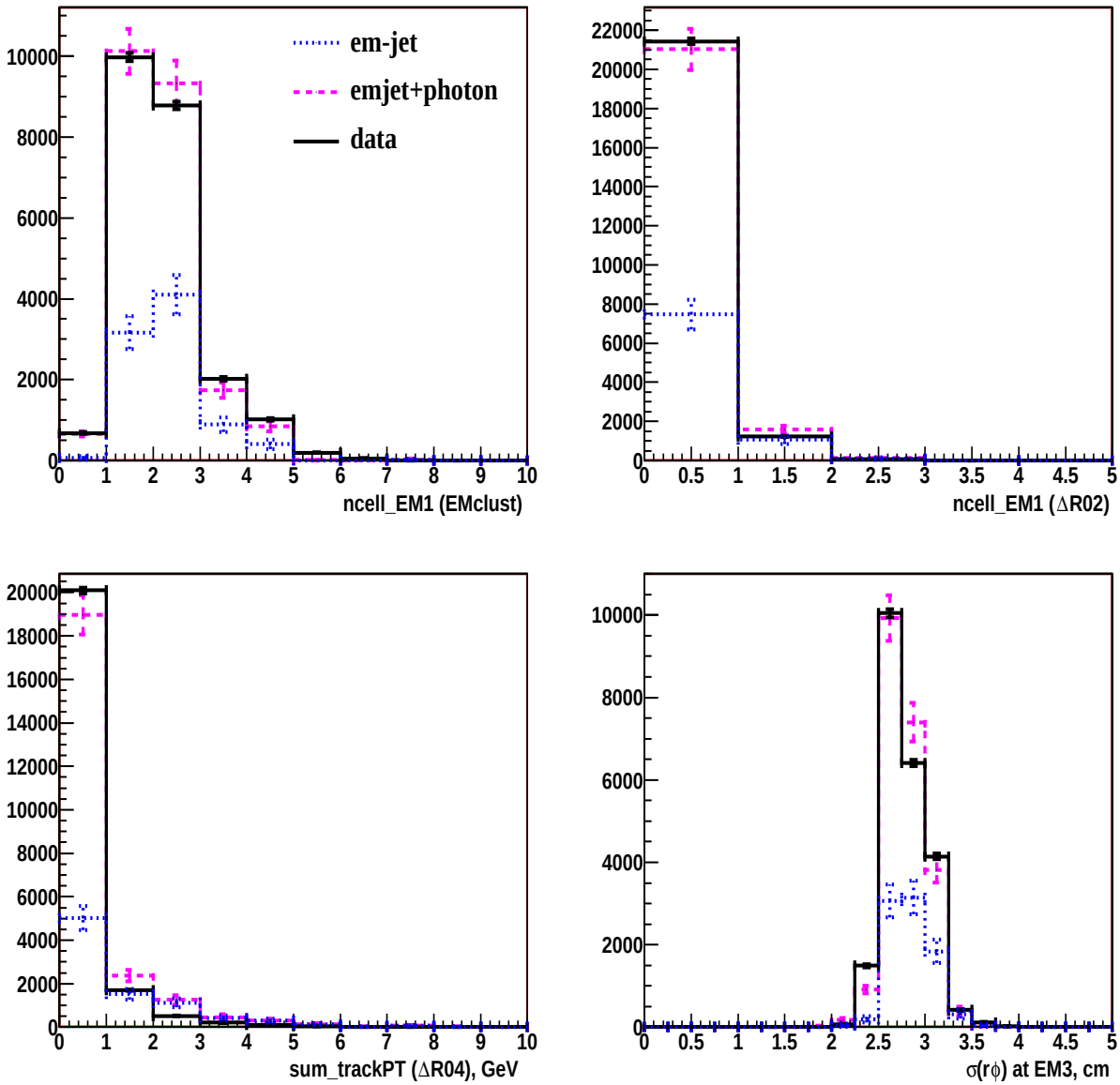

Figure 8: Same as in Fig. 1 but for $\mathbf{60} < \mathbf{p_T^\gamma} < \mathbf{70}$ GeV with $P = 0.640 \pm 0.043$.

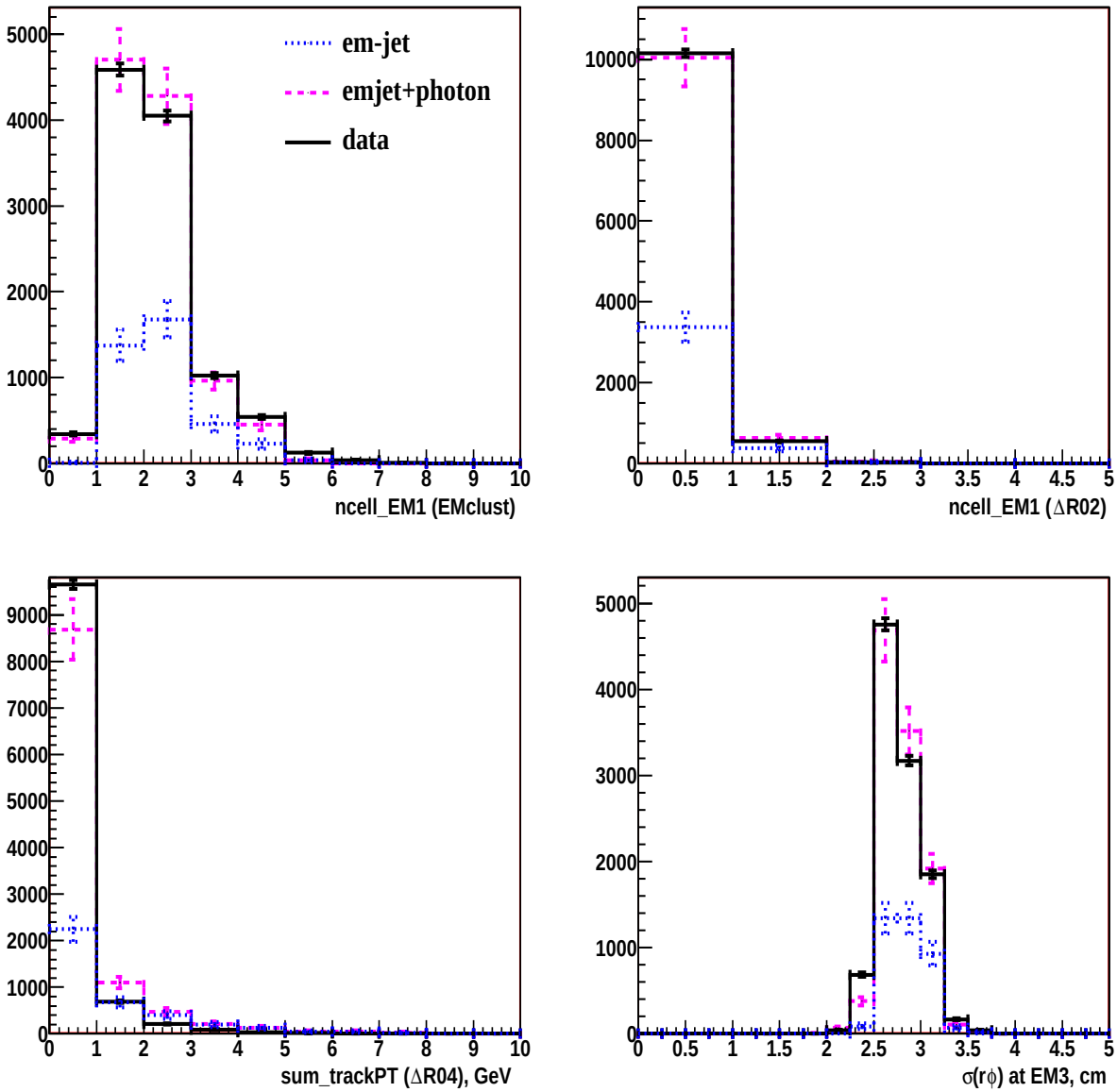

Figure 9: Same as in Fig. 1 but for $\mathbf{70} < \mathbf{p_T^\gamma} < \mathbf{80}$ GeV with $P = 0.647 \pm 0.059$.

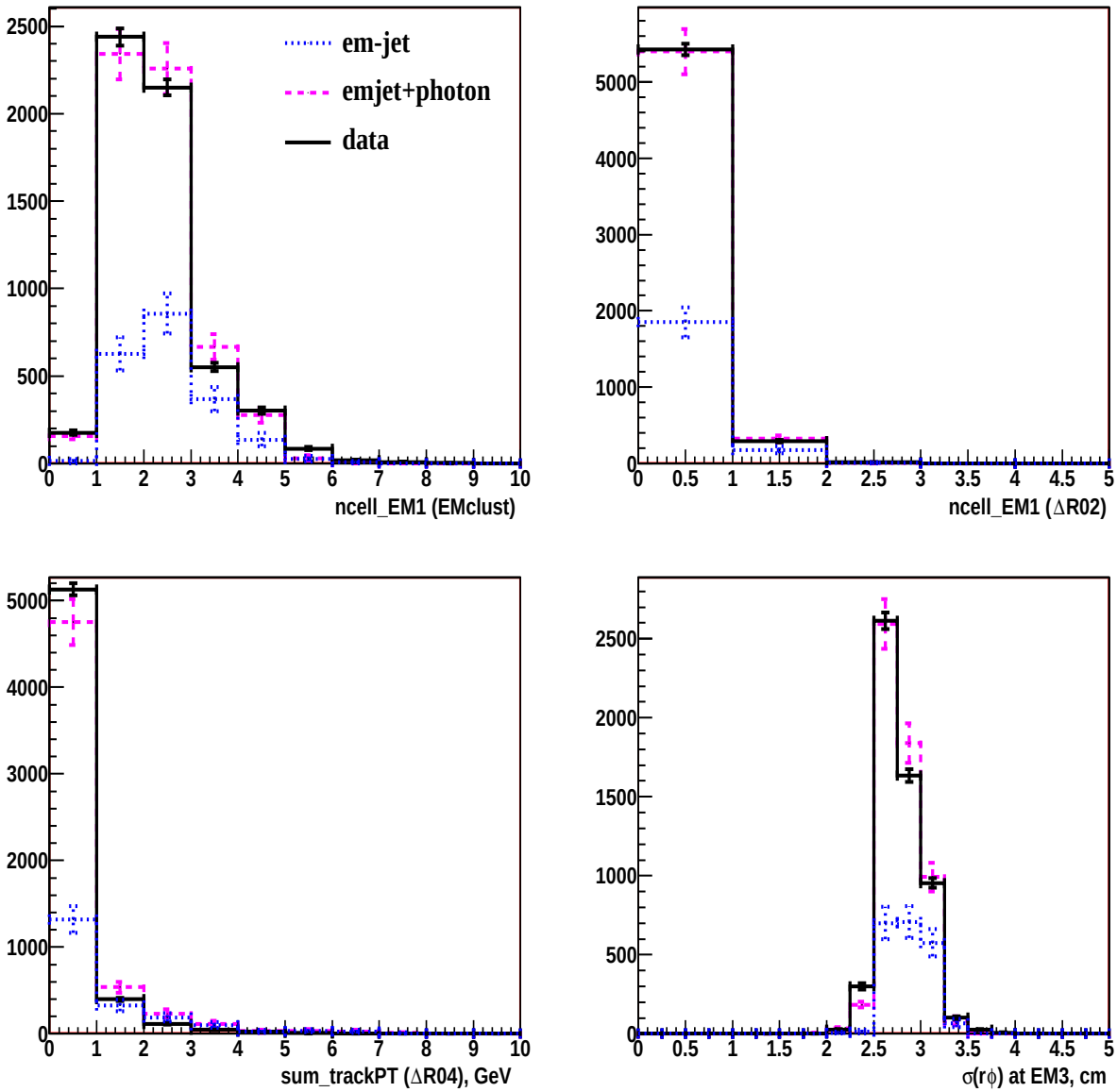

Figure 10: Same as in Fig. 1 but for $\mathbf{80} < \mathbf{p_T^\gamma} < \mathbf{90}$ GeV with $P = 0.645 \pm 0.050$.

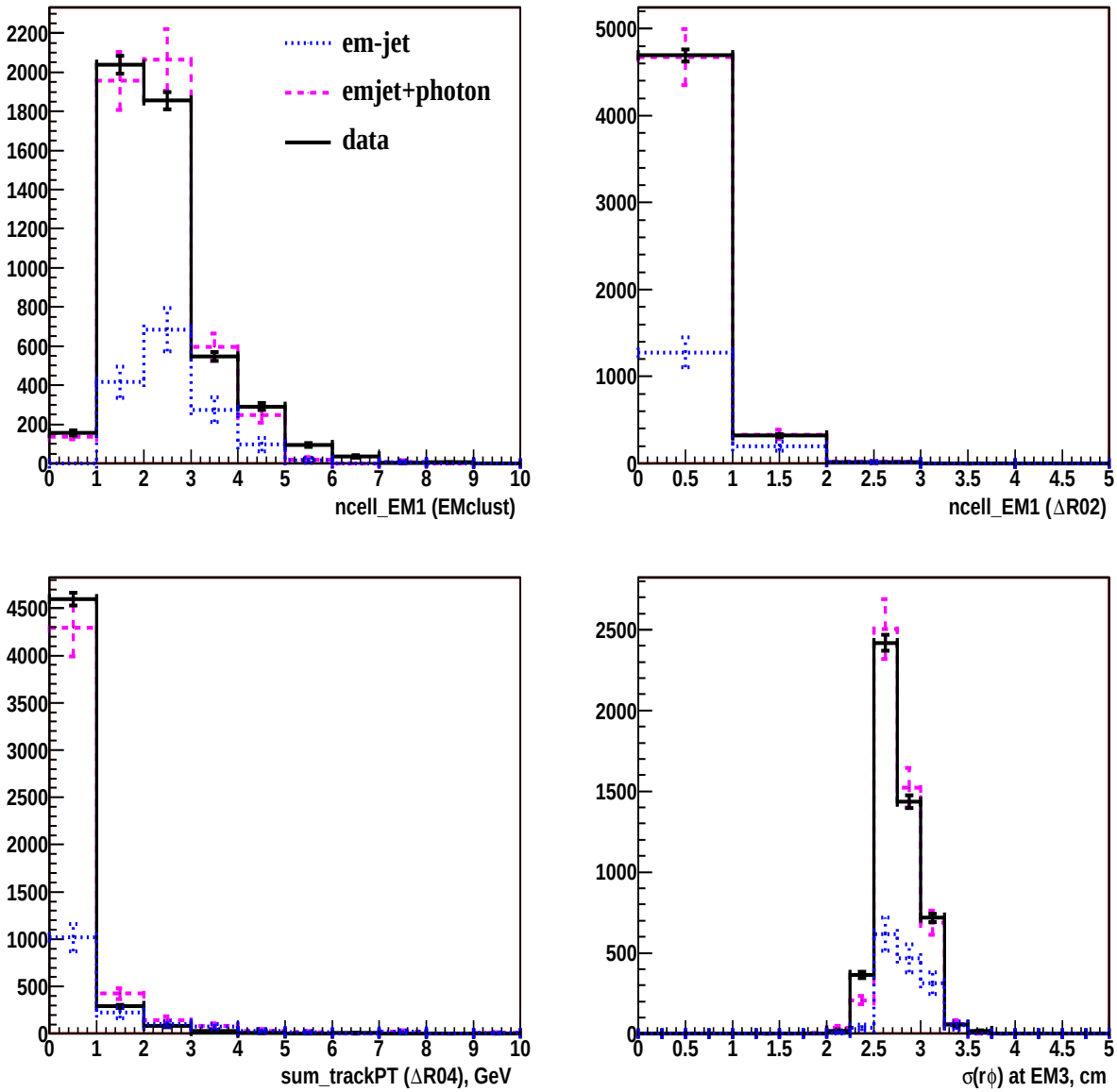

Figure 11: Same as in Fig. 1 but for $\mathbf{90} < \mathbf{p_T^\gamma} < \mathbf{110}$ GeV with $P = 0.704 \pm 0.056$.

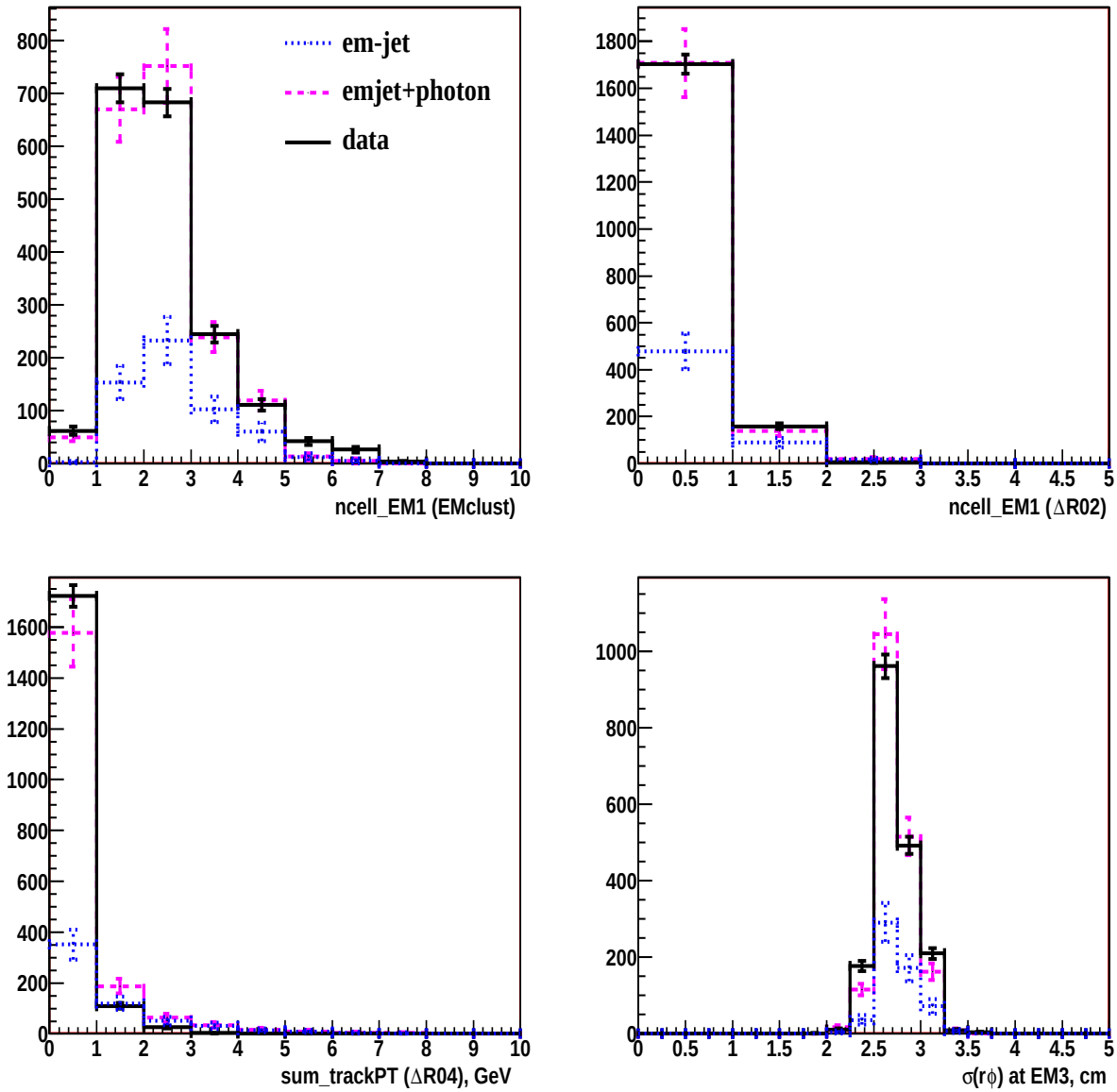

Figure 12: Same as in Fig. 1 but for $\mathbf{110} < \mathbf{p_T^\gamma} < \mathbf{130}$ GeV with $P = 0.678 \pm 0.068$.

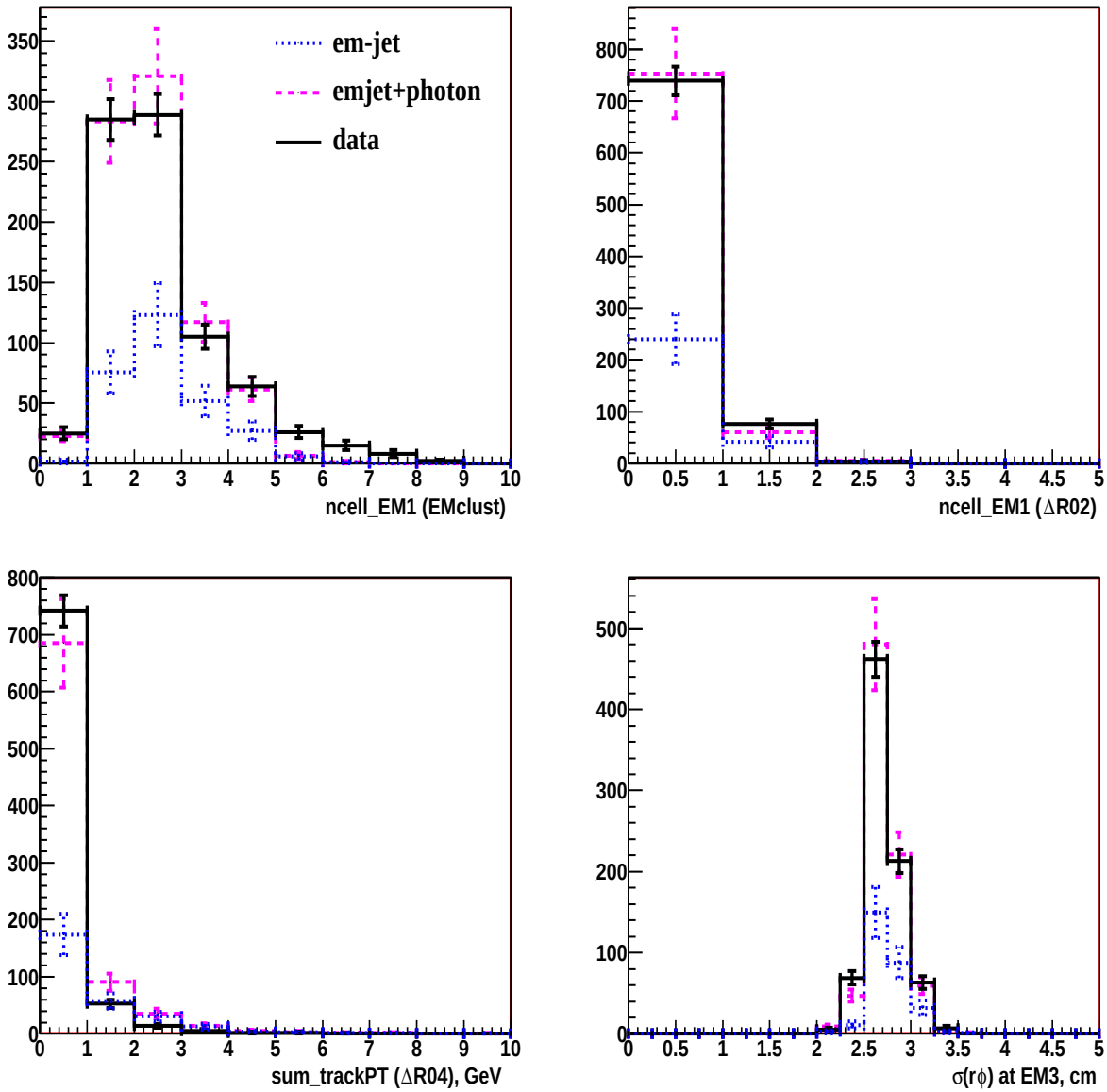

Figure 13: Same as in Fig. 1 but for $\mathbf{130} < \mathbf{p_T^\gamma} < \mathbf{150}$ GeV with $P = 0.685 \pm 0.089$.

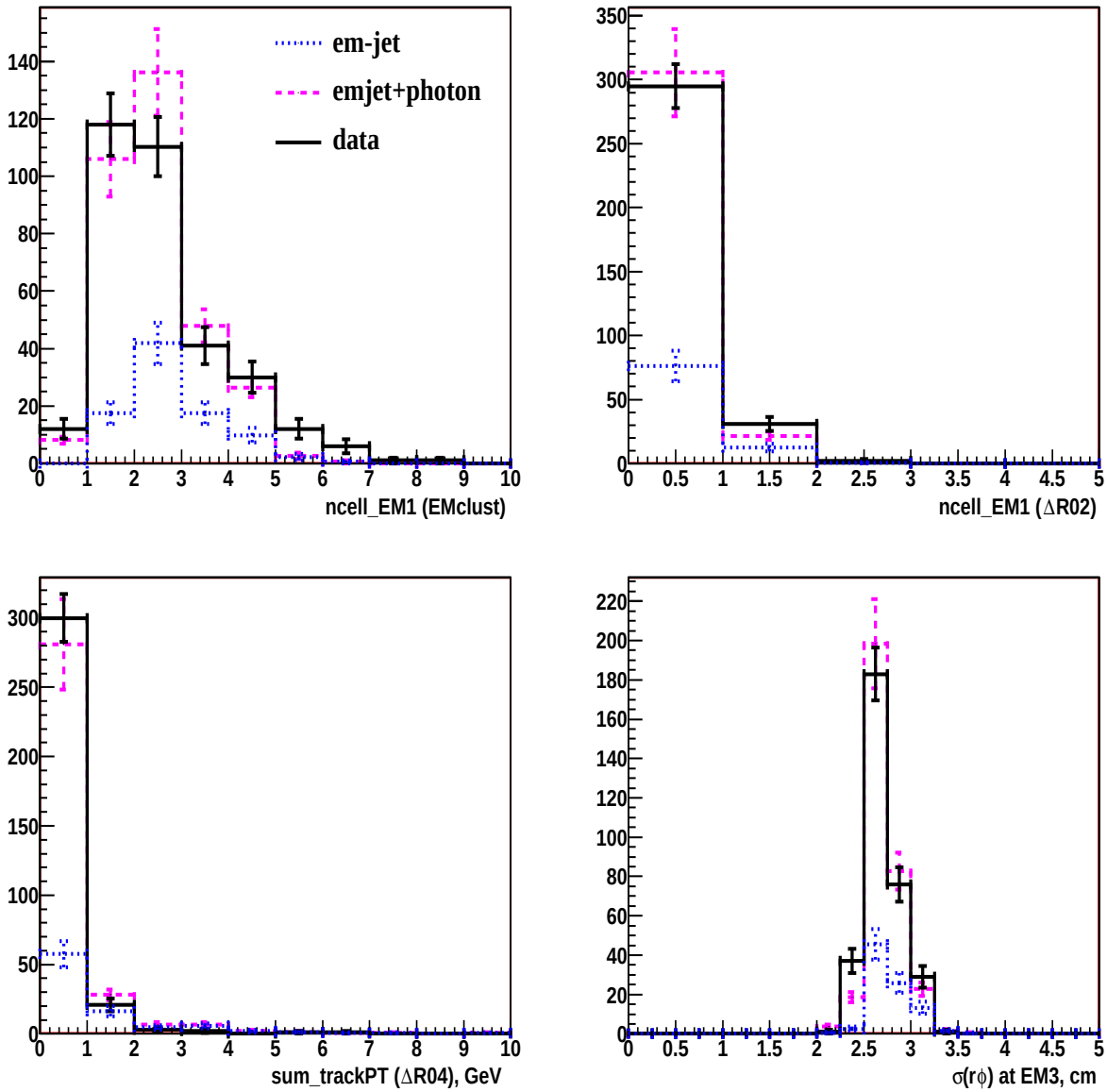

Figure 14: Same as in Fig. 1 but for $\mathbf{150} < \mathbf{p_T^\gamma} < \mathbf{170}$ GeV with $P = 0.727 \pm 0.101$.

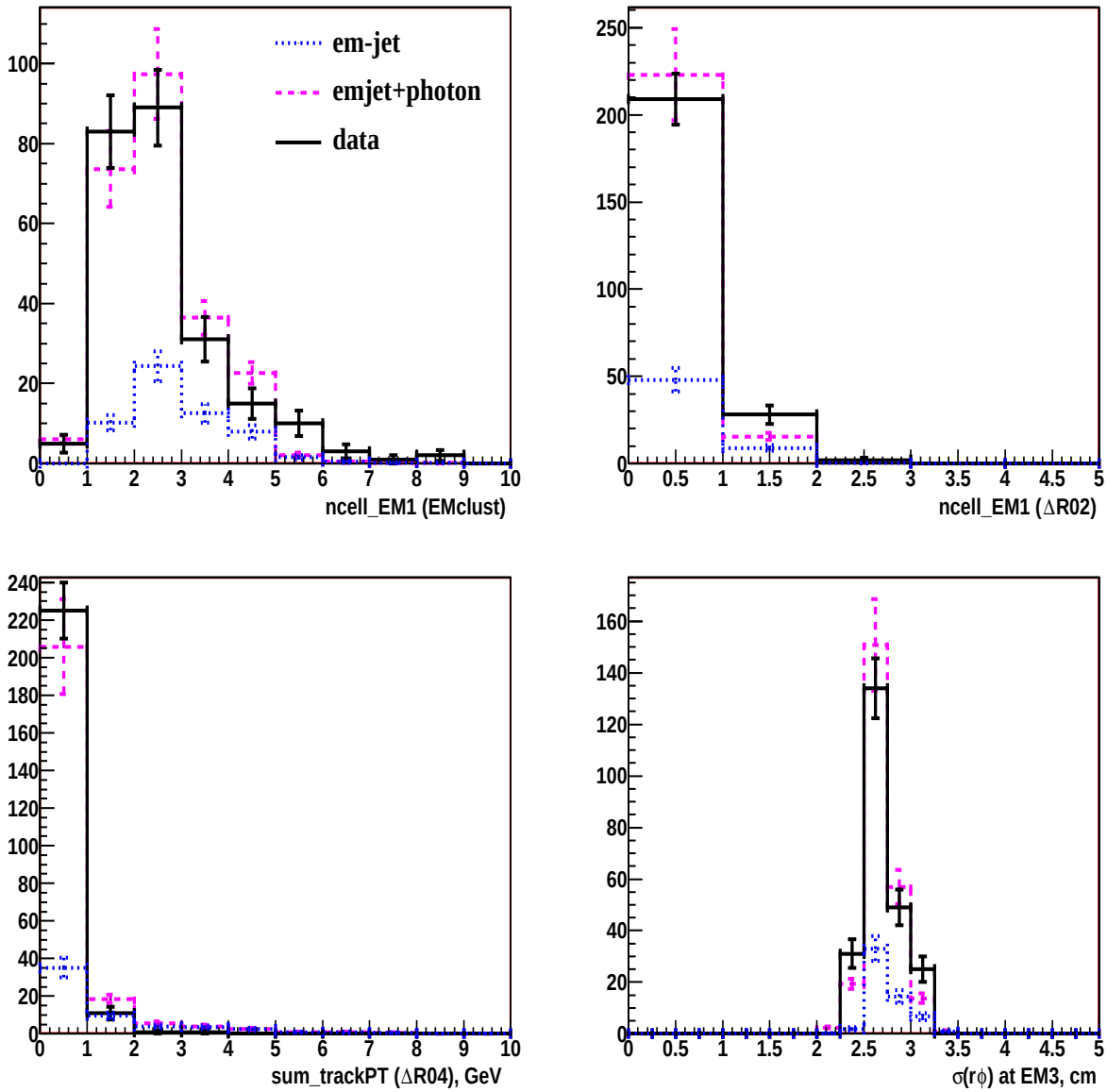

Figure 15: Same as in Fig. 1 but for $\mathbf{170} < \mathbf{p_T^\gamma} < \mathbf{200}$ GeV with $P = 0.761 \pm 0.110$.

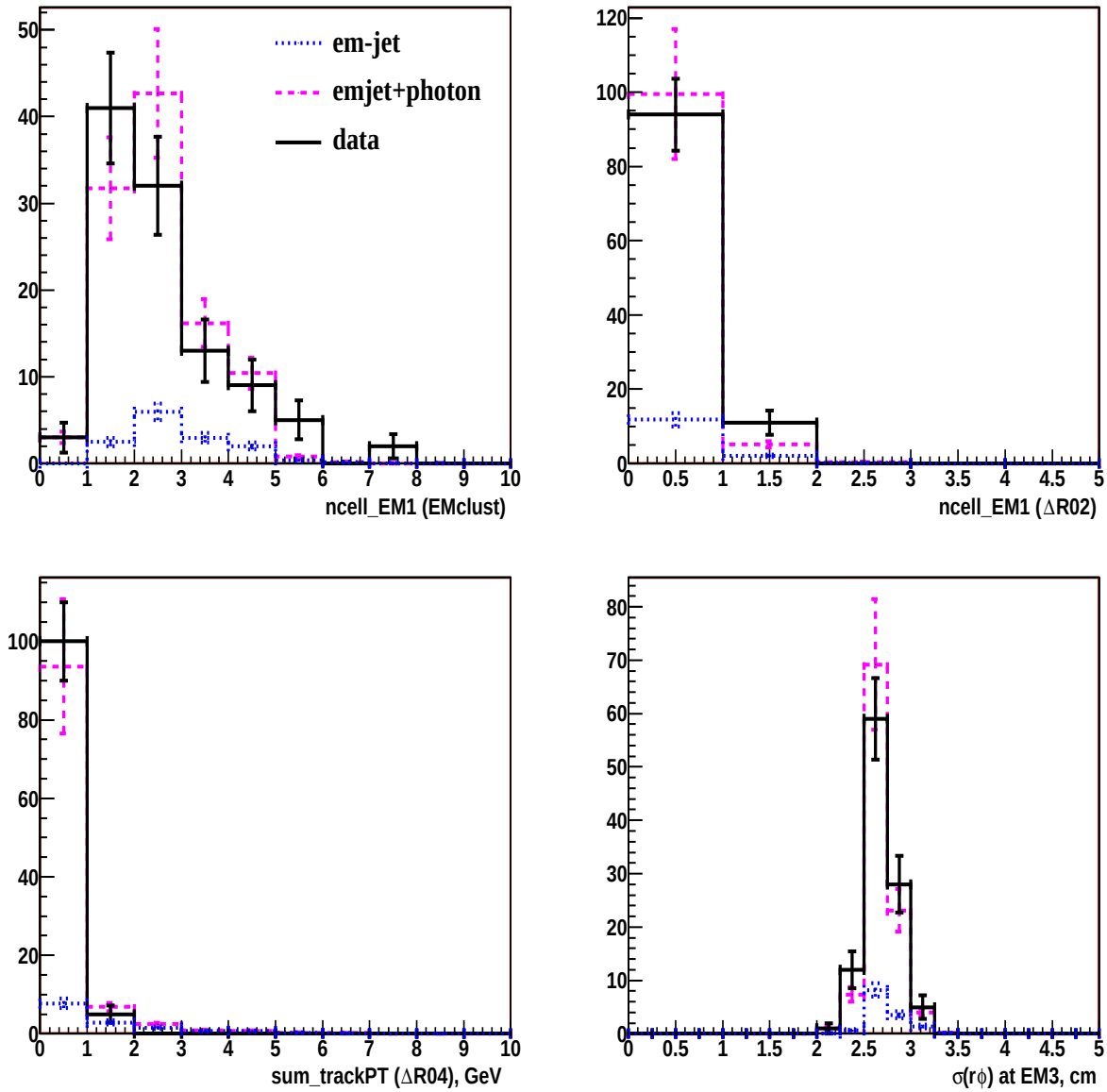

Figure 16: Same as in Fig. 1 but for $\mathbf{200} < \mathbf{p_T^\gamma} < \mathbf{230}$ GeV with $P = 0.847 \pm 0.172$.

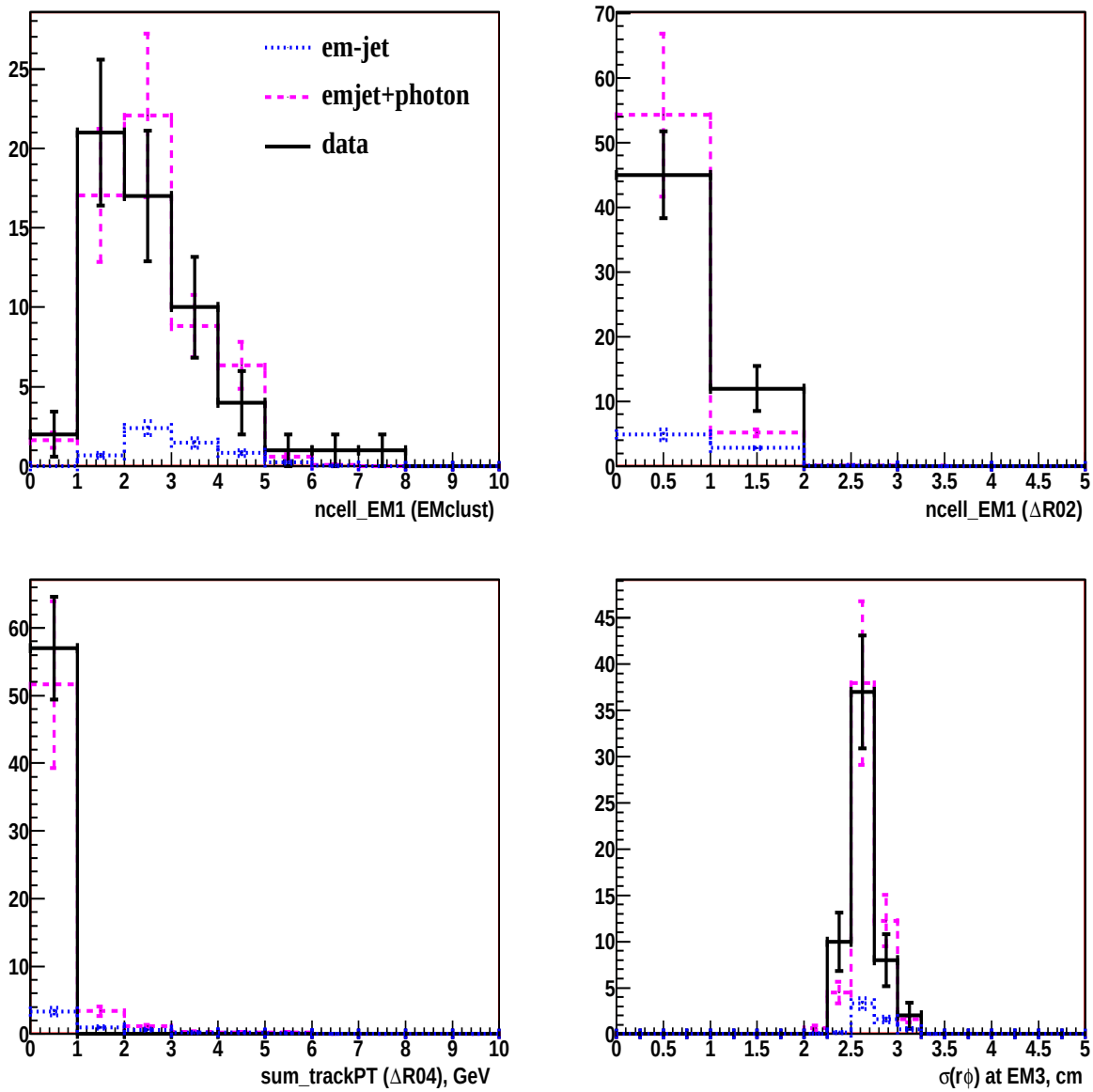

Figure 17: Same as in Fig. 1 but for $\mathbf{230} < \mathbf{p_T^\gamma} < \mathbf{300}$ GeV with $P = 0.901 \pm 0.228$.